

A COMMUNITY PALM MODEL

A PREPRINT

✉ Nicholas Clinton¹, ✉ Andreas Vollrath², ✉ Remi D’Annunzio², ✉ Desheng Liu³, ✉ Henry B. Glick⁴, ✉ Adria Descals⁵, ✉ Oliver Guinan¹, ✉ Alicia Sullivan¹, ✉ Jacob Abramowitz¹², ✉ Fred Stolle⁷, ✉ Chris Goodman⁸, ✉ Tanya Birch¹, ✉ David Quinn¹, ✉ Olga Danylo⁹, ✉ T. Lips¹⁰, ✉ Daniel Coelho¹, ✉ Enikoe Bihari¹¹, ✉ Bryce Cronkite-Ratcliff¹, ✉ Ate Poortinga¹¹, ✉ Atena Haghighattalab¹¹, ✉ Evan Notman¹², ✉ Michael DeWitt¹, ✉ Aaron Yonas¹, ✉ Gennadii Donchyts¹, ✉ Devaja Shah¹, ✉ David Saah¹¹, ✉ Karis Tenneson¹¹, ✉ Nguyen Hanh Quyen¹¹, ✉ Megha Verma⁴, and ✉ Andrew Wilcox⁴

¹Google LLC, Mountain View, CA, USA

²Food and Agriculture Organization of the United Nations, Rome, Italy

³Department of Geography, The Ohio State University, Columbus, OH, USA

⁴Unilever, Business Operations Sustainability, Englewood Cliffs, NJ, USA

⁵CREAF, Cerdanyola del Vallès, 08193 Barcelona, Spain

⁶University of Alabama, Huntsville, AL, USA

⁷World Resources Institute, Washington DC, USA

⁸NGIS, Perth, WA, Australia

⁹RESTOR, Fraumünsterstrasse 16, 8001 Zurich, Switzerland

¹⁰(personal capacity)

¹¹Spatial Informatics Group, Pleasanton, CA, USA

¹¹United States Agency for International Development, Washington DC, USA

¹²NASA SERVIR Science Coordination Office, Marshall Space Flight Center, Huntsville, AL, USA

November 6, 2024

ABSTRACT

Palm oil production has been identified as one of the major drivers of deforestation for tropical countries. To meet supply chain objectives, soft commodity producing companies and other stakeholders need timely information of land cover dynamics in their supply shed. However, such data are difficult to obtain from suppliers who may lack digital geographic representations of their supply sheds and production locations. There is also a proliferation of mapping products coming onto the market, which have a spectrum of methods, definitions and geographic extents that may present conflicting information and can quickly become outdated. Here we present a “community model,” a machine learning model trained on pooled data sourced from many different stakeholders, to produce a map of palm probability at global scale. An advantage of this method is the inclusion of varied inputs, the ability to easily update the model as new training data becomes available and run the model on any year for which input imagery is available. Inclusion of diverse data sources into one probability map can help establish a shared understanding across stakeholders on the presence and absence of a land cover or commodity (in this case oil palm). The model predictors are annual composites built from publicly available satellite imagery provided by Sentinel-1, Sentinel-2, and ALOS-2, and terrain data from Jaxa (AW3D30) and Copernicus (GLO-30). We provide map outputs as the probability of palm in a given pixel, to reflect the model certainty of the underlying state (palm or not palm). This version of this model provides global accuracy estimated to be 92% (at 0.5 probability threshold) on an independent test set. This model, and resulting oil palm probability map products are useful for accurately identifying the geographic footprint of palm cultivation. Used in conjunction with timely deforestation information, this palm model is useful for understanding the risk of continued oil palm plantation expansion in sensitive forest areas.

Keywords palm · community · model · remote sensing · machine learning · satellite · imagery

1 Introduction

Commodity supply chains have come to global attention in recent years, driven by heightened awareness of deforestation and its consequential CO₂ emissions resulting from land cover conversion [Pendrill et al., 2019, 2022]. This revelation has spurred voluntary commitments from major consumer packaged goods suppliers, exemplified by Unilever, which has pledged to pursue deforestation-free practices [Vijay et al., 2016]. Initiatives like the Round-table on Sustainable Palm Oil (RSPO) serve as proactive measures undertaken by industry stakeholders to address the environmental challenges associated with palm oil production. The urgency for accurate and timely information about commodity production locations has been further emphasized by recent regulations such as the European Union Deforestation Regulation (EUDR). Notably, the European Union identified palm oil as the primary driver of Union-driven deforestation among the eight commodities analyzed [European Commission, 2023].

EUDR, the United Kingdom’s Environment Act, and proposed bills like the US FOREST Act, are pushing deforestation-free commodity production from voluntary commitments to a regulatory requirement for doing business in global markets. In the case of the EUDR, this means organizations operating or placing products in the EU market must provide [European Commission, 2023]:

- Geo-referenced location(s) of commodity production (EUDR Article 9, European Commission 2023).
- A due diligence process that demonstrates that the locations from which commodities are sourced are at low risk of deforestation (EUDR Article 10, European Commission 2023).

The risk assessment portion of the due diligence process requires large-scale, wall-to-wall, robust, and regularly updated information on land cover and land use in order to ensure that deforestation is not occurring in the sourcing locations. Remote sensing and machine learning techniques offer promising methodologies for rapidly creating large scale land cover commodity datasets to support organizations’ due diligence reporting on their supply chains. Although commodity probability maps are not solely sufficient to ensure compliance, they are necessary to support organizations’ understandings of the impact of their supply chains, verify information provided by producers, and support due diligence reporting.

There are many land cover studies that result in high-quality maps, however they quickly go out of date and decision makers are tasked with selecting one of them, harmonizing them, or making a new one if they require maps for additional time periods, resolutions, or compliance with a particular regulation. Commercial providers also advertise commodity maps, but it can be difficult to obtain information on pricing, specifications on availability, accuracy and method of production, limiting their utility. Recognizing the importance of open, credible, up-to-date, and consistent data products, the Forest Data Partnership has developed a model for oil palm mapping that can be easily updated with new, community-supplied information. We consider the ability of local stakeholders to correct model output in their areas of knowledge to be an important element in the development of ethical, fair and representative models. This communal approach involves market participants, regulated entities, regulators, researchers, and NGOs, working in collaboration to create a unified and sustainable solution.

Palm oil is a primary source of edible vegetable oil globally, with approximately 79.5 million tons produced in 2024 [Service, 2024, Ritchie, 2021]. In the period from 2000 to 2018, the conversion of forest to oil palm contributed to 7% of global deforestation, with 29% in Asia and 11% in Oceania [FAO, 2022]. Geographically, palm oil production is concentrated within a narrow tropical band, predominantly in three Southeast Asian countries: Indonesia, Malaysia, and Thailand [Ritchie, 2021]. Indonesia alone accounts for 59% of global production [Service, 2024]. Consequently, the expansion of oil palm cultivation has emerged as the primary driver of deforestation in Indonesia [Austin et al., 2019]. Nonetheless, the rate of oil palm expansion in Indonesia peaked around 2010 and has since decreased [Gaveau et al., 2022]. The expansion rate of oil palm plantations in Indonesia closely mirrors the price of crude palm oil prices over time, with higher commodity prices fostering accelerated expansion [Gaveau et al., 2022, Xin et al., 2021].

Remote sensing-based mapping of oil palm is an area of active research. A combination of optical and synthetic aperture radar (SAR) data is often employed with a classifier, such as random forest, to outperform either data source alone [Nomura and Mitchard, 2018, Ordway et al., 2019, Descals et al., 2019, Sarzynski et al., 2020, Xu et al., 2020, Abramowitz et al., 2023]. Li et al. [2017] used auto-encoders on high resolution QuickBird imagery to detect and count individual oil palm trees in Malaysia. Working with Sentinel-1 and Sentinel-2 data, [Descals et al., 2021, 2024] used a convolutional neural network (CNN) to map oil palm globally, with distinction between industrial and smallholder plantations. Danylo et al. [2021] applied unsupervised methods to Landsat and Sentinel-1 data to map oil palm over time. In conjunction with maps constructed from remotely sensed imagery, Gaveau et al. [2018] and Gaveau et al. [2022] used manual delineation by experts to map oil palm.

The aim of this study is to leverage existing work and diverse data sources to develop a community supported Machine Learning (ML) model capable of generating annual oil palm maps from the most recent data available. Building on the

existing studies mentioned above, we used the published data (where available) from these and other sources to create a communal training/validation dataset and a community ML model – a model that can be employed on-demand to create oil palm maps for time periods and locations with suitable input data. The advantage of this type of model is that it leverages existing work, is inclusive of multiple datasets from multiple contributors, improves over time, leverages public imagery sources, doesn’t lead to a proliferation of competing products and gives consumers access to the means of map production. We characterize the accuracy of the community palm model, and show that estimated probabilities output by the model can be used in statistically-based decision making frameworks. Specifically, we use the model output at two points in time in a risk analysis framework, to quantify the risk of palm transitions in forested areas. This risk assessment is designed to elucidate the probability of palm conversion either from, or to, other land covers in the time and area of interest. We make the model, input data and output data available to the community for ongoing collaborative development.

2 Methods

The methods were chosen to help organizations understand the location of oil palm production, and change in such production over time as it relates to deforestation. The workflow is designed to be iterative, to facilitate rapid acquisition of additional training/validation data, model retraining and model deployment. To build this workflow, reference data were ingested into Google Earth Engine [Gorelick et al., 2017] from multiple sources, and then overlaid on geographic predictors (imagery) to create training and validation sets. A TensorFlow-based neural network [Abadi et al., 2015] was trained on the data and deployed to Google Vertex AI for inference at scale in Earth Engine. The model accuracy was assessed with the validation data. We performed a cross-source validation, which retrained the model leaving out one training dataset at a time to understand the contribution of each training set to the overall model performance. We also present a method to estimate risk of palm-driven deforestation by looking at predictions at two points in time for the same area.

2.1 Training/Testing data

A key to this approach is the ongoing community contribution of the training and testing data that we used to build the model. Initial data sources were provided by community contributors to the Forest Data Partnership. Accuracy improves over time as additional community members contribute data to the model, which can be easily republished and re-evaluated. The data described below are provisional, and we expect stakeholders to provide more data in their areas of interest, with commensurate increase in model accuracy in those areas. Additional data sources will be cited as new model versions are published.

Using Maxar WorldView-3 for visual reference, Google collected 8054 1024x1024 patches at 0.3 meter resolution at nadir, independently hand-labeled by two separate annotators. Oil Palm was described to annotators as “oil palm trees planted in rows or terraces for agricultural purposes.” Bare ground patches of yet-to-be-planted palm plantations were not labeled as palm.

These were sampled to generate 326,714 points at 10 meter resolution of palm frequency in $[0, 1]$ based on the proportion of the 10 meter pixel annotated as palm or not-palm by both annotators. These annotations were performed on recent imagery available at the time of annotation, and were assumed to fairly represent 2021 conditions. Palm plantations operate on a growth and replanting cycle of approximately 25 years, leading to the assumption that annotation of imagery from a few years prior to 2021 would generally reflect the state of palm in 2021.

Vollrath et al. [2019] provided 5,145 patches as 120x120 meter polygons representing palm in 2017. These patches were sampled and pooled to produce 738,421 points at 10 meter resolution: palm (1) or not palm (0).

Publicly available validation data from Danylo et al. [2021] were downloaded from their GitHub site in the form of 10,303 palm presence (1) or absence (0) points (in 30x30 meter patches). These resulted in 10,265 10-meter samples of palm (1) or not palm (0) in 2017.

T. Lips (*personal communication*) provided 180 labeled points according to palm presence or absence in 2023. These were hand-digitized using an earlier version of the model output as reference. Specifically, points of palm presence were placed in areas of obvious under-prediction (false negatives) and points of palm absence were placed in areas of obvious over-prediction (false positives).

Publicly available data for palm plantations in Peru for 2019-2020 were obtained from Fricker et al. [2022] in the form of 1288 polygons. These data were combined with tree cover masks, a stable forest mask, the Descals et al. [2021] palm mask and subsampling (0.005 rate) at 10 meter resolution to produce 6469 palm (1) presence points.

Publicly available validation data from Descals et al. [2024] were downloaded from their Zenodo site (<https://zenodo.org/records/13379129>) in the form of 18,812 palm presence (1) or absence (0) points (in 10x10 meter patches). These resulted in 18,736 10-meter samples of palm (1) or not palm (0) in 2021. These data were not used for training or model selection.

To balance the training data, pseudo-absence points (assumed not palm locations) were generated from ancillary layers on forest cover and land cover. Specifically, Dynamic World [Brown et al., 2022] was used to find stable non-tree areas, defined as majority non-tree classes over a three year period (2019-2021). Multiple forest datasets were combined to estimate stable, non-plantation, forest cover over the observation period (1984-2020). Palm pseudo-absences were generated by stratified sampling of stable non-tree and stable forest areas in the following regions: Southeast Asia (n=14,124), Central America (n=9624), West Africa (n=35,145), and Peru (n=7819).

2.2 Predictor data

The predictors are annual composites built from publicly available satellite imagery provided by Sentinel-1, Sentinel-2, and ALOS-2, and terrain data from Jaxa (AW3D30) and Copernicus (GLO-30). Specifically, the following Sentinel-2 Top-of-atmosphere (TOA) reflectance bands were used: B1, B2, B3, B4, B5, B6, B7, B8, B8A, B9, B10, B11, B12. TOA reflectance data were used due to the increased availability of TOA data compared to data products with a higher level of processing, surface reflectance for example. We built annual composites by taking the cloud-masked pixel- and band-wise mean for all available imagery in a calendar year. The Cloud Score+ dataset [Pasquarella et al., 2023] was used for the cloud mask, with a 0.6 threshold on the 'cs_cdf' band. The means were scaled to reflectance in approximately [0, 1] and no further normalization was performed.

Sentinel-1 data were selected from interferometric wide-swath scenes that included both VV (vertical-vertical) and VH (vertical-horizontal) polarizations in both ascending and descending orbital paths. Radiometric compensation for terrain using the volume scattering model described by Vollrath et al. [2020] was used to preprocess backscattering coefficients. For a calendar year, minimum, maximum, mean, and standard deviation of backscatter were computed at each polarization and subsequently stretched to decibels.

Palsar-2 annual composites, containing HH and HV polarizations at 25 meters resolution [Shimada et al., 2014], were bilinearly resampled, gap filled with the rolling 3-year mean of annual composites, and converted to scaled decibels.

Slope was derived from the ALOS AW3D30 digital surface model, a global, 30-meter surface model provided by JAXA [Tadono et al., 2016, Takaku et al., 2016]. Slopes were scaled to [0, 1] with no further normalization.

In a given calendar year, the eight Sentinel-1 statistics (min, max, mean, and SD for both VV and VH) were stacked with the 13 Sentinel-2 band means, the two Palsar-2 bands (HH and HV) and slope to create the annual input composites.

The palm datasets described above were combined with composites from the relevant years to produce 979,585 multi-temporal training/testing points spanning 59 countries and 10 biomes [Dinerstein et al., 2017], with class distribution:

- 575,893 negatives (not palm)
- 532,467 positives (palm)

The pooled data were geographically partitioned into three folds based on a hexagonal decomposition of an equal-area projection, where each cell was roughly 26,000 square kilometers. See Goldblatt et al. [2018] and Fairfax et al. [2023] for a detailed description of this decomposition. Because the total boundary length of a hexagonal partition is minimized, we chose this method to minimize spatial autocorrelation between training, testing validation data. The size and label balance of the folds vary slightly, a property we leveraged by choosing the largest fold for training. Of the remaining two folds, one was used for model selection and hyperparameter tuning (validation) and the other for evaluation (i.e. not used in model training or selection).

The geographic distribution of positive (palm=1) and negative (palm=0) reference points is illustrated in Figure 1. The distribution of over a portion of Southeast Asia are illustrated in Figure 2.

2.3 Model training and inference

The model is a neural network with four hidden layers and a single sigmoid output. It is a per-pixel model in which the input is $1 \times 1 \times C$ (for C bands) vector and the output ($F(x_t)$) is the estimated conditional probability of palm presence given the vector of covariates (x_t) at time t . The architecture, activation function, optimization function, learning rate, batch size, training iterations and other parameters of the model and training configuration were



Figure 1: Location of training/testing reference locations: negatives (white), positives (gray).

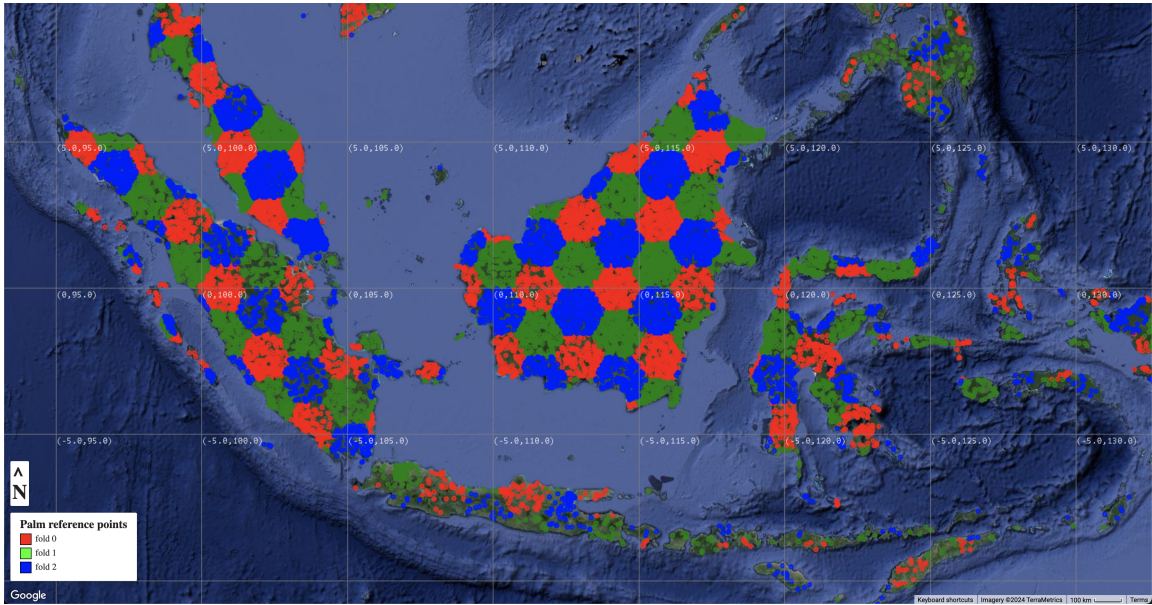


Figure 2: Distribution of folds: fold 0 (red), fold 1 (green), fold 2 (blue)

Table 1: Palm indicators at two points in time

$t-1 = 2020$	$t = 2023$	
	$P_{2023} = 1$	$P_{2023} = 0$
$P_{2020} = 1$	$p11 = P(P_{t-1}=1, P_t=1)$	$p10 = P(P_{t-1}=1, P_t=0)$
$P_{2020} = 0$	$p01 = P(P_{t-1}=0, P_t=1)$	$p00 = P(P_{t-1}=0, P_t=0)$

chosen automatically using a hyperparameter search performed on infrastructure similar to Google Cloud AutoML (<https://cloud.google.com/automl>).

Model inference was performed for 2020 and 2023, where the inputs to the model were determined by compositing the predictors on an annual basis. This time frame was chosen to roughly coincide with the EUDR baseline (2020) and the most recent complete calendar year of data.

2.4 Model accuracy assessment

We estimate overall map accuracy in two ways. We used the test fold (not seen in training or model selection/tuning) to compute the following accuracy measures: binary cross-entropy loss, binary overall accuracy at 0.5 threshold of output, area under the receiver operator characteristics (ROC) curve (AUC) [Fawcett, 2006], recall and precision at 0.5 threshold on the output. As noted in [Zhao et al., 2014], "self-evaluation" is a notorious overestimate of map accuracy. We also use Descals et al. [2024] validation data to compute the same measures (all folds and only folds 0 and 1, which are not in the same geographic fold as the training data). The Descals et al. [2024] training or validation data were not used in model training or selection.

2.5 Risk assessment

Here we define risk as the sum of potential land cover transitions times their associated probabilities in a region of interest (ROI). To-palm is the transition of non-palm land cover to palm in any pixel, in units of pixel area. From-palm is the transition from palm to any non-palm land cover in any pixel, in units of pixel area. We categorize land cover into two categories: forest and non-forest, according to Bourgoin et al. [2023]. We define the probability of the to-palm transition as $P(P_{t-1} = 0, P_t = 1)$ where P is the probability operator, and P_t (italicized) is a Bernoulli distributed random variable that indicates palm presence (1) or absence (0) at time t . The probability of the to-palm transition is the probability of not palm at time $t - 1$ and palm at time t .

The pair of Bernoullis at two points in time (P_{t-1}, P_t) is a bivariate Bernoulli distributed random variable [Marshall and Olkin, 1985, DAI et al., 2013]. Denote the probability of each possible state according to the contingency Table 1:

Note that $p11 + p10 + p01 + p00 = 1$ and that the marginal probability

$$P(P_{2023}) = P(P_{2020}, P_{2023}) + P(\sim P_{2020}, P_{2023}) = p11 + p01 \quad (1)$$

where \sim is the negation operator, i.e. $\sim P_{2020} == (P_{2020}=0)$.

The objective is to obtain $p01 = P(\sim P_{2020}, P_{2023}) = P(P_{2020} = 0, P_{2023} = 1)$. We treat the output of the model as an estimate of the parameters of the marginal Bernoulli distribution(s) in each pixel, i.e. $F(x_t) \approx P(P_t)$ for some t . With $F(x_t) \approx P(P_t)$ as an estimate of the marginal $P(P_{2023})$, we need an estimate of $p11$ to obtain $p01$ from equation 1.

Assume that the Spearman correlation $(F(x_{t-1}), F(x_t))$ in a spatio-temporal neighborhood (i.e. the correlation computed in a 310x310 meter, 31x31 pixel, neighborhood centered on each pixel in the image inputs) is a fair approximation to the Pearson correlation of the unknown indicator variables. Note that the Pearson correlation is defined as:

$$\rho_{t-1,t} = (E[P_{t-1} * P_t] - E[P_{t-1}] * E[P_t]) / ((\text{Var}(P_{t-1}) * \text{Var}(P_t))^{1/2}) \quad (2)$$

where E is the expectation operator and Var is the variance operator. Note that we have estimates of the marginal expectations (e.g. $F(x_t)$) and variances (e.g. $F(x_t)(1 - F(x_t))$) from the model. Also note that $E[P_{t-1} * P_t] = P(P_{t-1} = 1, P_t = 1) = p11$, so we can estimate $p11$ from the estimate of spatio-temporal correlation. As a result, we can estimate $p01$ as



Figure 3: Annual (2020) mean composite of Sentinel-2 bands B4, B3, B2 as red, green, blue respectively.

Table 2: Accuracy measures on multiple datasets.

Accuracy Measure	Test fold	Descals et al. 2024
Cross-entropy loss	0.097	0.183
Binary accuracy @ 0.5 threshold	0.969	0.924
Area under the ROC curve (AUC)	0.992	0.976
Recall @ 0.5 threshold	0.968	0.913
Precision @ 0.5 threshold	0.969	0.600

$$p01 = P(\text{to-palm}) = P(P_t) - \rho_{t-1,t} * (F(x_t)(1 - F(x_t))F(x_{t-1})(1 - F(x_{t-1})))^1/2 + F(x_t)F(x_{t-1}) \quad (3)$$

Note that we can also estimate p10 (P(from-palm)) by substituting P_{t-1} for P_t in equation 3. We define the cost of a transition as the area (hectares) of a pixel ($A_{i,j}$) in which a transition occurred. The risk of transition associated with a given ROI is therefore the sum over all i, j in the ROI of $A_{i,j} * P(\text{transition})_{i,j}$.

3 Results

Figures 3-6 show 2020 annual composites of the predictors in the model at a specific location.

The model is published as a trained TensorFlow model on GitHub (<https://github.com/google/forest-data-partnership>). For interactive display and/or further analysis, the model can be hosted on platforms like Google Vertex AI and model output accessed from Google Earth Engine.

For palm producing countries, annual probability maps for 2020 and 2023 are produced as 10m raster image collections that are available in the Google Earth Engine public data catalog under a CC-BY 4.0 NC license for non-commercial users and commercial licensing by request (see Section 6). Figures 6-7 shows the model output (estimated conditional probabilities) for years 2020 and 2023.

3.1 Accuracy

Table 2 shows accuracy measures computed from the geographic test fold and folds 0 and 2 of the Descals et al. [2024] validation set. Binary accuracy (threshold = 0.5) is approximately 92% on the holdout data.

The accuracy assessment illustrates several important issues. The test fold consistently shows higher accuracy than the Descals et al. [2024] validation set, suggesting potential self-evaluation bias and/or dependence between folds. Since

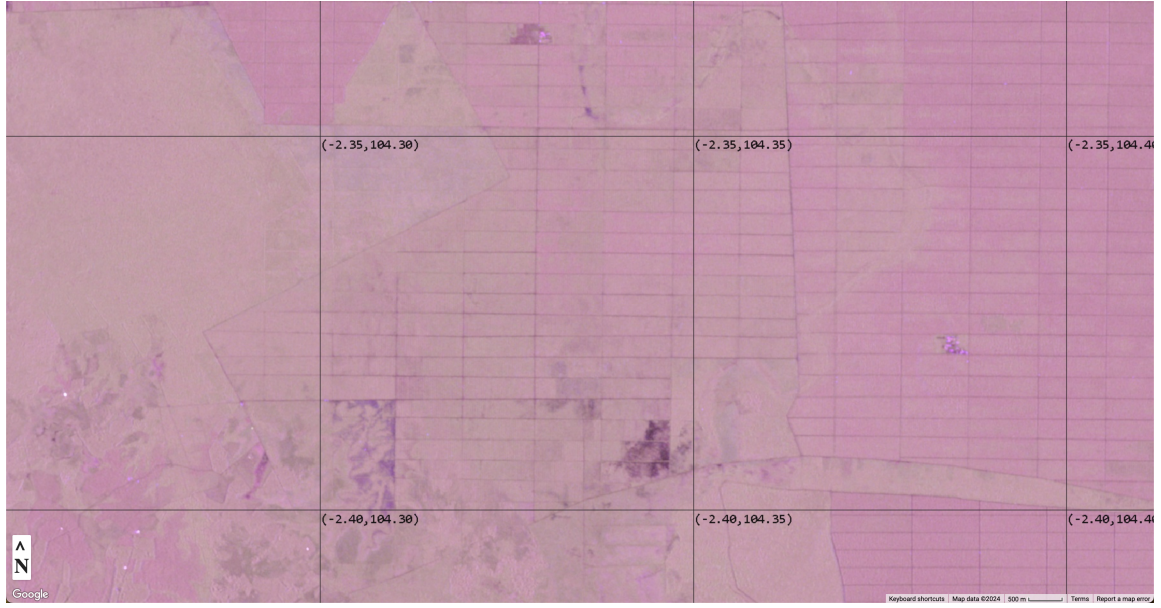


Figure 4: Annual (2020) mean composite of Sentinel-1 bands VV mean, VH mean, VV standard deviation as red, green, blue.

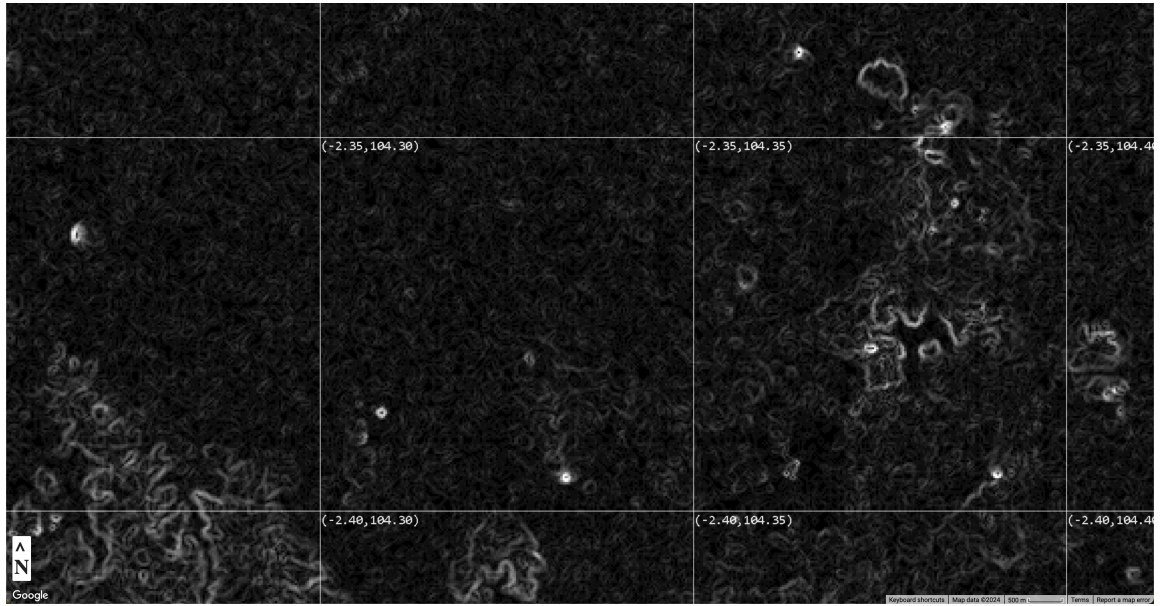


Figure 5: Slope derived from ALOS AW3D30 (low to high slope: black to white).

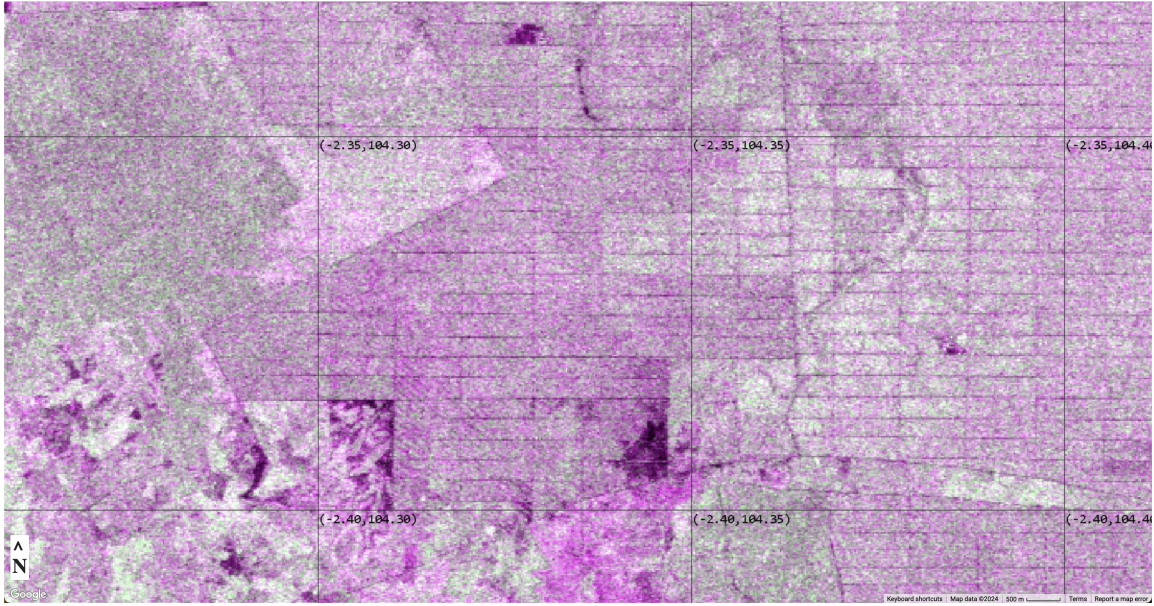


Figure 6: Annual (2020) Palsar-2 composite, HH, HV, HH bands as red, green blue.

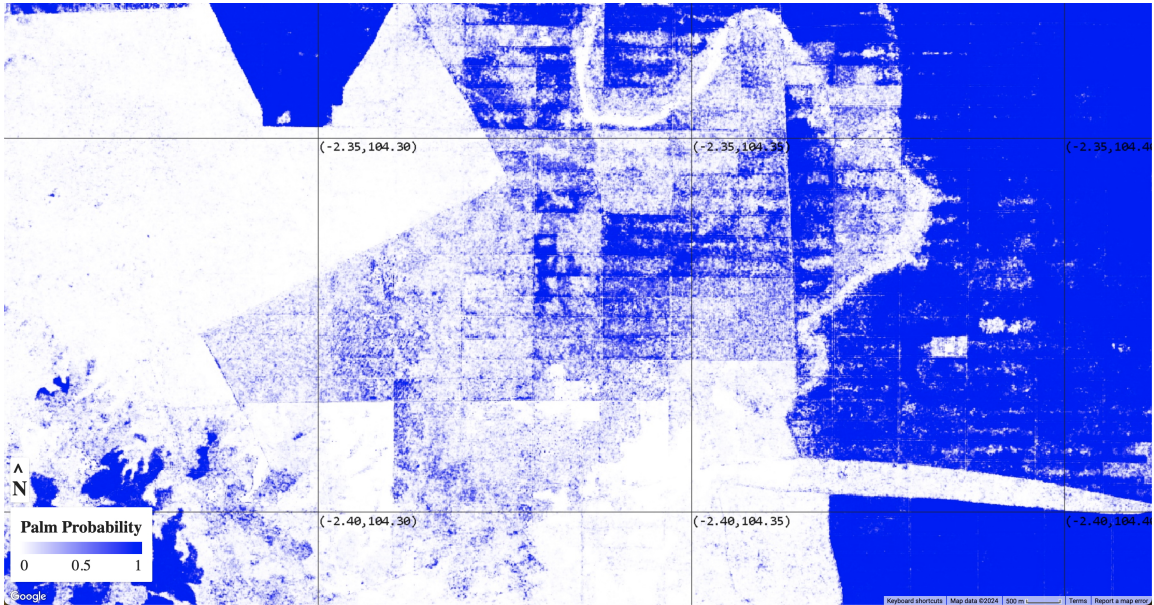


Figure 7: Estimated palm probability 2020.

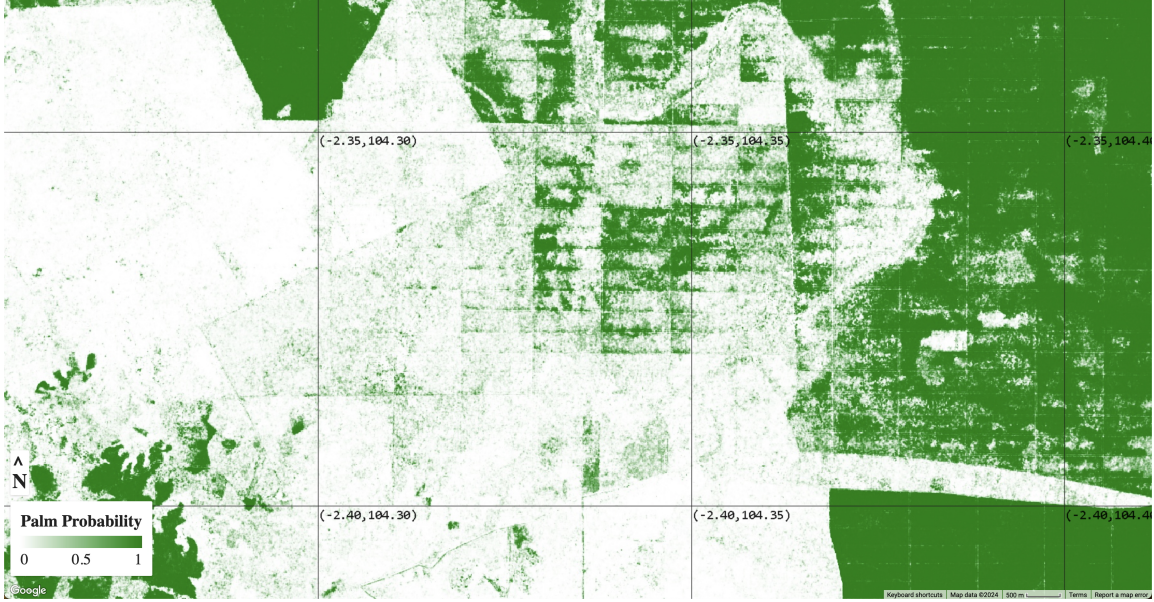


Figure 8: Estimated palm probability 2023.

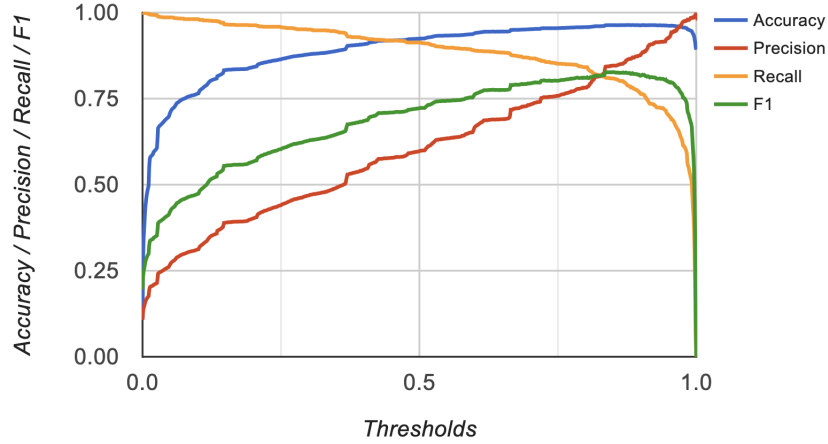


Figure 9: Accuracy, F1, precision and recall curves on Descals et al. 2024 validation data.

the Descals et al. [2024] validation data were not seen in model training or selection, and were restricted to geographic locations different from the training data, these are a more conservative estimate of overall model performance. Note that the precision at threshold 0.5 is 60% on this set, suggesting overestimation in non-palm areas at low thresholds. Figure 9 shows overall accuracy, F1, precision and recall curves for the model on the Descals et al. [2024] validation set. Note that the threshold which optimizes F1 score is closer to 0.82, where precision and recall are 82%. Figure 9 also illustrates the extreme imbalance (towards negatives) of the the Descals et al. [2024] validation set. Specifically, overall accuracy increases with increasing threshold, which is near 96% at the 0.82 threshold.

3.2 Risk assessment

Figure 10 shows the estimated probability of palm transitions from years 2020 to 2023, computed according to equation 3 or its analog for P_{t-1} . The three regions shown in Fig. 10 correspond to hypothetical sourcing domains. Inspection of the imagery suggests that region 1 (red) represents an area without palm, the region 2 (green) represents a mixed area, and region 3 (blue) represents an established palm plantation. The risk of palm transition associated with each ROI was computed as the sum of estimated probability of the transition in each pixel times cost of the transition (pixel area in hectares). The results are shown in Table 3.

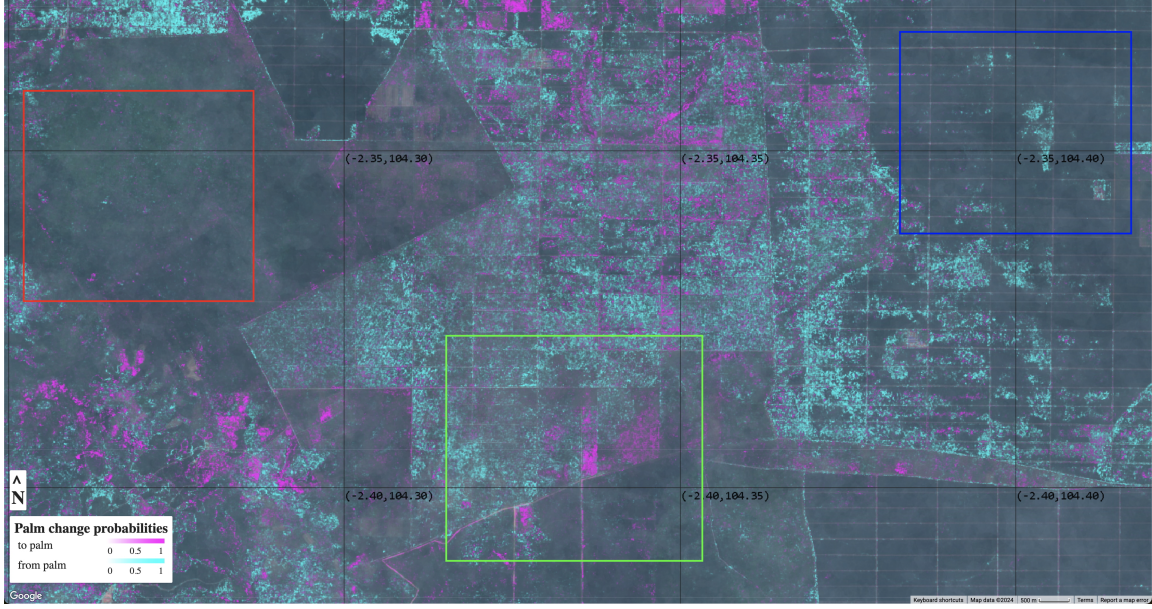


Figure 10: Hypothetical sourcing domains and palm transition probabilities, with 2023 Sentinel-2 RGB background.

Table 3: Transition risk in forest categories.

Areas (ha)	Region 1	Region 2	Region 3
Forest	983	102	0
To-palm risk (forest)	17.9	2.4	N/A
From-palm risk (forest)	14.9	1.7	N/A
Non-forest	331	1465	1266
To-palm risk (non-forest)	5.1	83.6	4.8
From-palm risk (non-forest)	5.3	126.5	32.9

4 Discussion

The method described here leverages existing datasets to create a model applicable to any time or place given sufficient input data. This is important in the context of regulatory processes that require harmonization of potentially ambiguous information to demonstrate sustainability. A community model is useful for a logical, data-driven approach to model probability of existence of a specific commodity at a certain location. This approach is of ever increasing importance due to the proliferation of maps and the need for companies to demonstrate compliance with existing and emerging nature protection laws. Specifically, regulations intended to ensure commodities are not sourced from recently deforested places require the disambiguation of conversion of natural forest to commodity production from other kinds of forest management.

Interpreting the model output as probabilities retains local uncertainty in the underlying condition, which is unknown. The global oil palm probability map developed with this method can be a two-class (palm versus not-palm) classification by thresholding probabilities using automatic methods such as Otsu segmentation [Otsu, 1979]. The threshold determined by Otsu for the 2023 palm map (roughly the area of Figure 10) is 0.506. Thresholding the 2023 palm in Figure 7 at 0.506 indicates 5842 hectares of planted palm in the area of Figure 10. From Table 2, recall is relatively high at a 0.5 threshold, but precision is low. Any selected threshold represents a trade-off between recall and precision as shown in Figure 9. For this reason, it is incumbent on the user of the data to determine a threshold suitable for their use case and region of interest, for example using Otsu segmentation to select an optimal threshold for local conditions. However, threshold delineation is not required, as the probabilities can be used directly. Treating the probabilities as an estimated distribution over the unknown (and assumed hidden) Bernoulli random variable (Palm: 0, 1), indicates 6317 hectares of planted palm in Figure 7 – an 8% difference compared to the threshold method.

Since the contingency table can be specified completely with the assumptions described previously, it can be used to generate estimates of the probability of different scenarios while accounting for uncertainty in model estimates at

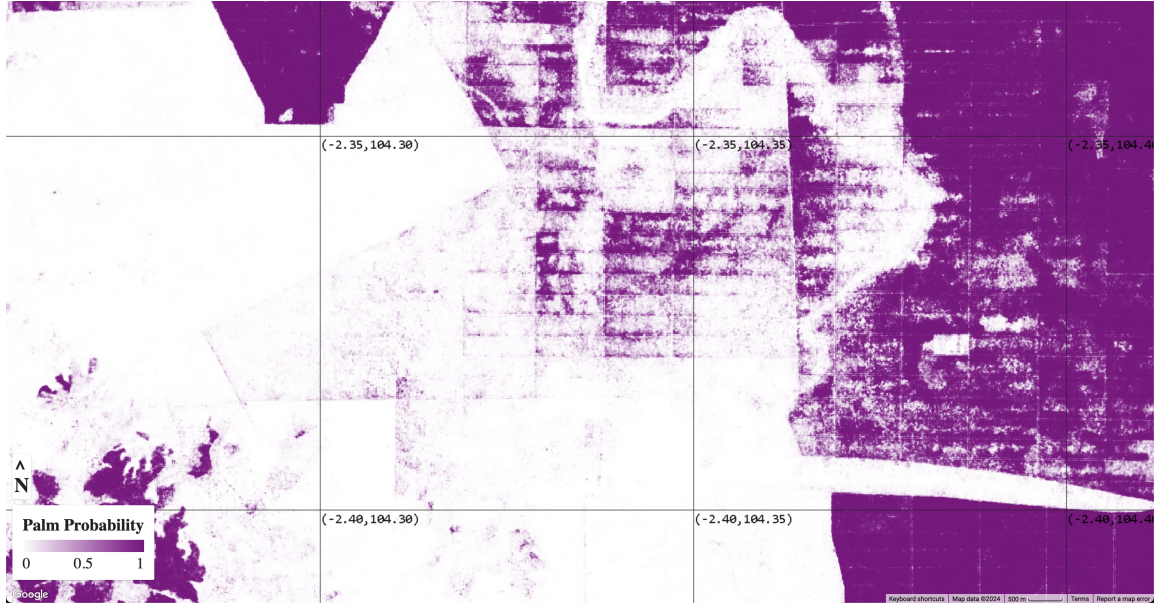


Figure 11: Estimated palm probability: both 2020 and 2023.

multiple points in time. For example, the estimate of p_{11} is the probability of "stable" palm, or places that were palm in both 2020 and 2023 (Figure 11). Estimates of persistent palm seem less noisy than single year output, but additional testing is required to confirm that. Risk can be computed for any scenario, in units of area, using the method described. Although risks computed in this manner can be used directly in supply chain analysis, due to potential model error, the risks should be interpreted with caution. Specifically, these data can indicate the need for additional verification or characterization of high risk areas, but should be combined with other evidence to establish risk definitively.

For example, consider the three regions in Figure 10 and Table 3. In region 1, the majority of the area is in forest, as defined by Bourgoin et al. [2023]. Although the to-palm risk is 18 hectares, there is also from-palm risk of 15 hectares. In region 1, we conclude that the model output is noisy, as the from-palm transition risk roughly balances the to-palm transition risk. In region 2, there is some forest, and small amounts of transition risk, which we conclude to be either noise or active palm plantation management. Region 3 is all non-forest. In region 3, there are relatively high amounts of transition, which we assume to be palm management. We don't interpret any of these areas as particularly high risk. Limitations of this approach are discussed below.

For such a model to be effective in meeting sustainability commitments, oil palm maps must be produced on a yearly basis, since compliance is determined annually. The model also needs to be easy to update, meaning that stakeholders can contribute data in their areas of interest, if the model output is not representative of that area. This is especially important from an ethical perspective, where local stakeholders need inclusion in a process that could affect their livelihoods. Further verification of submissions may be required where submissions are found to reduce overall or local model accuracy. A single iteration of the process consists of an examination of model results by a relevant stakeholder, creation of additional training/validation data in the stakeholder's ROI, model refinement and retraining using the new data, and publication of the updated model. That workflow was demonstrated here. Specifically, preliminary model results were provided to T. Lips, who created a new training dataset, after which point the improved model was retrained and republished. Additional iterations and version tracking are needed to keep the model inclusive, accurate and up-to-date.

4.1 Limitations

Although uncertainty is implicit in the model output, which is expressed as a probability, the model could be biased due to training data biases or an inability to generalize the training data in the model weights. This bias could be reduced through enhancements to model architecture, for example through inputting spatio-temporal patches of inputs instead of single pixel vectors from annual composites. There could also be high variance in the model output. This is illustrated by the analysis of region 1, in which noise in model output is assumed to account for a substantial amount of from- and to-palm transitions in the region. Variance could be reduced through collection of a more geographically representative and balanced training data set. We suspect variance is also reduced by combining multiple years of predictions to isolate

stable crops of interest (e.g. Figure 11), but additional research is needed to confirm that suspicion. Presently, known limitations resulting from model bias and/or variance mean quality of predictions will vary geographically and results should be interpreted with caution.

The probabilistic framework on which the risk assessment is based relies on strong assumptions. We assume that the true state of a pixel can be adequately represented by a Bernoulli random variable, implying that a pixel can be in only one of two states: palm or not palm. We make little effort to determine, or even to define, such states, which are simply taught to the model directly from the data. Given a vector of predictors, we assume the model output is a suitable representation of the conditional probability of oil palm at a given location, and treat it as the marginal probability of the unknown indicator variable. Finally, the estimate of palm conversion depends on the estimation of correlation of the unknown indicators from the Spearman rank correlation of the model outputs. The Spearman correlation is probably an overestimate of the Pearson correlation between the unknown indicators, since the rank-correlation can be high for non-linearly related variables. This would overestimate p11 and consequently underestimate the transition risk.

4.2 Future Work

We intend for the model presented here to continuously improve. To maximize effectiveness, the model should evolve as relevant community stakeholders contribute additional data. To this end, we invite the larger community of local, regional, and global stakeholders to submit informed feedback, additional training data and/or other information (feedback form: <https://goo.gle/fdap-data>). Improvements are not limited to a steadily increasing amount of training and/or validation data. The model could be improved through changes in input format (e.g. patches, which contain more spatial information) and/or model architecture. The inputs could be improved through incorporation of more information as new sensors come online or through learned embedding spaces ([Jean et al., 2019]). Community contributions to model and/or input data are welcome through our GitHub repository (see Section 6). We expect modeling other land covers of interest (e.g. cocoa, coffee, rubber) in a community framework to increase accuracy and availability of information about the spatio-temporal distribution of commodities and relationship to deforestation.

5 Conclusion

We have presented a “community model” approach to generate open, timely, consistent and global land cover maps for oil palm production. The strength of this approach comes from cross stakeholder data pooling for training, ease of incorporating additional training data over time and the open availability of the trained machine learning models and probability maps. The community land cover model we present here can be operated at multiple points in time and/or multiple geographic locations and can take multiple diverse inputs.

This model, and resulting oil palm probability maps are useful for accurately identifying the geographic footprint of oil palm cultivation, and how that footprint is changing over time. We have demonstrated how the analysis of the model outputs at multiple points in time can be used to infer oil palm dynamics. We recognize that the commodity probability maps are not solely sufficient to quantify palm oil driven deforestation, however they are necessary to disambiguate deforestation of natural forests from other kinds of land cover transitions. Used in conjunction with other geospatial information, such as global forest cover, deforestation alerts and high resolution imagery, this community palm oil map and risk indicators will support organizations’ understanding of the impact of their supply chains, help to verify information provided by producers, and support due diligence reporting. Specifically for regulatory mechanisms like the EUDR, we intend for the community model and resulting data products to support the “convergence of evidence” approach developed by the Forest Data Partnership for due diligence statements and compliance claims.

Ongoing research and development is needed to continue to refine the community palm model and map products. Additionally, expansion of the community model method to commodities beyond palm is needed to sufficiently characterize how commodity production is changing over time and impacting the world’s remaining forests.

6 Model and Data

Interactive palm oil probability viewer:

<https://forestdatapartnership.projects.earthengine.app/view/palm>

Trained models and model hosting example:

<https://github.com/google/forest-data-partnership/tree/main>

Earth Engine asset:

`ee.ImageCollection("projects/forestdatapartnership/assets/palm/model_2024a")`

7 Acknowledgements

We would like to acknowledge USAID funding of the Forest Data Partnership. Matt Hancher provided a valuable review.

References

- Florence Pendrill, U. Martin Persson, Javier Godar, and Thomas Kastner. Deforestation displaced: trade in forest-risk commodities and the prospects for a global forest transition. *Environmental Research Letters*, 14(5), 2019. doi:10.1088/1748-9326/ab0d41.
- Florence Pendrill, U. Martin Persson, Thomas Kastner, and et al. Disentangling the numbers behind agriculture-driven tropical deforestation. *Science*, 377:eabm9267, 2022. doi:10.1126/science.abm9267.
- V. Vijay, S. L. Pimm, C. N. Jenkins, and S. J. Smith. The impacts of oil palm on recent deforestation and biodiversity loss. *PLoS ONE*, 11(7):e0159668, 2016. doi:10.1371/journal.pone.0159668.
- European Commission. Regulation of the european parliament and of the council on the making available on the union market and the export from the union of certain commodities and products associated with deforestation and forest degradation and repealing regulation (eu) no 995/2010, 2023. URL <https://data.consilium.europa.eu/doc/document/PE-82-2022-INIT/en/pdf>. Viewed 20240228.
- USDA Foreign Agricultural Service. Commodity explorer, 2024. URL <https://ipad.fas.usda.gov/cropeexplorer/cropview/commodityView.aspx?cropid=4243000>. Accessed 4/16/2024.
- Hannah Ritchie. Palm oil. Our World in Data, 2021. URL <https://ourworldindata.org/palm-oil>. Accessed 4/16/2024.
- FAO. Fra 2020 remote sensing survey: Vol. no. 186, 2022.
- K. G. Austin, A. Schwantes, Y. Gu, and P. S. Kasibhatla. What causes deforestation in indonesia? *Environmental Research Letters*, 14(2):024007, 2019. doi:10.1088/1748-9326/aaf6db.
- D. L. A. Gaveau, B. Locatelli, M. A. Salim, Husnayaen, T. Manurung, A. Descals, A. Angelsen, E. Meijaard, and D. Sheil. Slowing deforestation in indonesia follows declining oil palm expansion and lower oil prices. *PLOS ONE*, 17(3):e0266178, 2022. doi:10.1371/journal.pone.0266178.
- Y. Xin, L. Sun, and M. C. Hansen. Biophysical and socioeconomic drivers of oil palm expansion in indonesia. *Environmental Research Letters*, 16(3):034048, 2021. doi:10.1088/1748-9326/abce83.
- Keiko Nomura and Edward Mitchard. More than meets the eye: Using sentinel-2 to map smallholder plantations in complex forest landscapes. *Remote Sensing*, 10(11):1693, 2018. doi:10.3390/rs10111693.
- Elsa M. Ordway, Rosamond L. Naylor, Rodney N. Nkongho, and Eric F. Lambin. Oil palm expansion and deforestation in southwest cameroon associated with proliferation of informal mills. *Nature Communications*, 10(1):114, 2019. doi:10.1038/s41467-018-07915-2.
- Adrià Descals, Zoltan Szantoi, Erik Meijaard, Harsono Sutikno, Guruh Rindanata, and Serge Wich. Oil palm (*elaeis guineensis*) mapping with details: Smallholder versus industrial plantations and their extent in riau, sumatra. *Remote Sensing*, 11(21):2590, 2019. doi:10.3390/rs11212590.
- Tomasz Sarzynski, Xinyi Giam, Luis Carrasco, and Jonathan S. H. Lee. Combining radar and optical imagery to map oil palm plantations in sumatra, indonesia, using google earth engine. *Remote Sensing*, 12(7):1220, 2020. doi:10.3390/rs12071220.
- Yue Xu, Le Yu, Weijia Li, Philippe Ciais, Yan Cheng, and Peng Gong. Annual oil palm plantation maps in malaysia and indonesia from 2001 to 2016. *Earth System Science Data*, 12(2):847–867, 2020. doi:10.5194/essd-12-847-2020.
- Jessica Abramowitz, Evan Cherrington, Rebecca Griffin, Rebecca Muench, and Francis Mensah. Differentiating oil palm plantations from natural forest to improve land cover mapping in ghana. *Remote Sensing Applications: Society and Environment*, 30, 2023. doi:10.1016/j.rsase.2023.100968.
- Weijia Li, Haohuan Fu, Le Yu, and Arthur Cracknell. Deep learning based oil palm tree detection and counting for high-resolution remote sensing images. *Remote Sensing*, 9(1):22, 2017. doi:10.3390/rs9010022.

- Adrià Descals, Serge Wich, Erik Meijaard, David L. A. Gaveau, Susannah Peedell, and Zoltan Szantoi. High-resolution global map of smallholder and industrial closed-canopy oil palm plantations. *Earth System Science Data*, 13: 1211–1231, 2021. doi:10.5194/essd-13-1211-2021.
- A. Descals, D. L. A. Gaveau, S. Wich, Z. Szantoi, and E. Meijaard. Global mapping of oil palm planting year from 1990 to 2021. *Earth System Science Data Discussions*, 2024:1–24, 2024. doi:10.5194/essd-2024-157. URL <https://essd.copernicus.org/preprints/essd-2024-157/>.
- Olena Danylo, Johannes Pirker, Grégoire Lemoine, and et al. A map of the extent and year of detection of oil palm plantations in indonesia, malaysia and thailand. *Scientific Data*, 8(1):96, 2021. doi:10.1038/s41597-021-00867-1.
- David L. A. Gaveau, Ben Locatelli, Mohammad A. Salim, Hidayat Yaen, Pablo Pacheco, and Douglas Sheil. Rise and fall of forest loss and industrial plantations in borneo (2000–2017). *Conservation Letters*, 12(3):e12622, 2018. doi:10.1111/conl.12622.
- Noel Gorelick, Matt Hancher, Mike Dixon, Simon Ilyushchenko, David Thau, and Rebecca Moore. Google earth engine: Planetary-scale geospatial analysis for everyone. *Remote Sensing of Environment*, 202:18–27, 2017. ISSN 0034-4257. doi:<https://doi.org/10.1016/j.rse.2017.06.031>. URL <https://www.sciencedirect.com/science/article/pii/S0034425717302900>. Big Remotely Sensed Data: tools, applications and experiences.
- Martín Abadi, Ashish Agarwal, Paul Barham, and et al. Tensorflow: Large-scale machine learning on heterogeneous systems, 2015. URL <https://zenodo.org/records/10798587>. Software available from tensorflow.org.
- Andreas Vollrath, Jennifer Adams, Sara Aparicio, and John Mrziglod. A global palm oil map for the year 2017 using multi-sensor sar imagery, 2019. URL <https://nikal.eventsair.com/NikalWebsitePortal/living-planet-symposium-2019/lps19/Agenda/AgendaItemDetail?id=d5c77654-1c5e-45af-92b6-cebdcde7eca4>. Living Planet Symposium. ESA/ESRIN, Frascati, Italy.
- Geoffrey Fricker, Kylee Nielsen, Isabella Clark, Jaxson Davis, Sarah Bates, Isabella Davis, and Naira Pinto. Palm Oil Polygons for Ucayali Province, Peru (2019-2020), 2022. URL <https://doi.org/10.7910/DVN/BSC9EI>.
- Christopher Brown, Steven Brumby, Brookie Guzder-Williams, Tanya Birch, Samantha Hyde, Joseph Mazzariello, Wanda Czerwinski, Valerie Pasquarella, Robert Haertel, Simon Ilyushchenko, Kurt Schwehr, Mikaela Weisse, Fred Stolle, Craig Hanson, Oliver Guinan, Rebecca Moore, and Alexander Tait. Dynamic world, near real-time global 10 m land use land cover mapping. *Scientific Data*, 9:251, 06 2022. doi:10.1038/s41597-022-01307-4.
- Valerie J. Pasquarella, Christopher F. Brown, Wanda Czerwinski, and William J. Rucklidge. Comprehensive quality assessment of optical satellite imagery using weakly supervised video learning. In *Proceedings of the IEEE/CVF Conference on Computer Vision and Pattern Recognition (CVPR) Workshops*, pages 2125–2135, 2023.
- Andreas Vollrath, Adugna Mullissa, and Johannes Reiche. Angular-based radiometric slope correction for sentinel-1 on google earth engine. *Remote Sensing*, 12(11):1867, 2020. doi:10.3390/rs12111867.
- Masanobu Shimada, Takuya Itoh, Takeshi Motooka, Manabu Watanabe, Tomohiro Shiraishi, Rajesh Thapa, and Richard Lucas. New global forest/non-forest maps from alos palsar data (2007–2010). *Remote Sensing of Environment*, 155: 13–31, 2014. ISSN 0034-4257. doi:<https://doi.org/10.1016/j.rse.2014.04.014>. URL <https://www.sciencedirect.com/science/article/pii/S0034425714001527>.
- T. Tadono, H. Nagai, H. Ishida, F. Oda, S. Naito, K. Minakawa, and H. Iwamoto. Initial validation of the 30 m-mesh global digital surface model generated by alos prism. In *The International Archives of the Photogrammetry, Remote Sensing and Spatial Information Sciences, ISPRS*, volume XLI-B4, pages 157–162, 2016. URL <https://isprs-archives.copernicus.org/articles/XLI-B4/157/2016/isprs-archives-XLI-B4-157-2016.pdf>.
- J. Takaku, T. Tadono, K. Tsutsui, and M. Ichikawa. Validation of 'aw3d' global dsm generated from alos prism. In *ISPRS Annals of the Photogrammetry, Remote Sensing and Spatial Information Sciences*, volume III-4, pages 25–31, 2016. URL <https://isprs-annals.copernicus.org/articles/III-4/25/2016/isprs-annals-III-4-25-2016.pdf>.
- Eric Dinerstein, David Olson, Anup Joshi, Carly Vynne, Neil D. Burgess, Eric Wikramanayake, Nathan Hahn, Suzanne Palminteri, Prashant Hedao, Reed Noss, Matt Hansen, Harvey Locke, Erle C Ellis, Benjamin Jones, Charles Victor Barber, Randy Hayes, Cyril Kormos, Vance Martin, Eileen Crist, Wes Sechrest, Lori Price, Jonathan E. M. Baillie, Don Weeden, Kierán Suckling, Crystal Davis, Nigel Sizer, Rebecca Moore, David Thau, Tanya Birch, Peter Potapov, Svetlana Turubanova, Alexandra Tyukavina, Nadia de Souza, Lilian Pintea, José C. Brito, Othman A. Llewellyn, Anthony G. Miller, Annette Patzelt, Shahina A. Ghazanfar, Jonathan Timberlake, Heinz Klöser, Yara Shennan-Farpón, Roeland Kindt, Jens-Peter Barnekow Lillesø, Paulo van Breugel, Lars Graudal, Maianna Voge, Khalaf F. Al-Shammari, and Muhammad Saleem. An ecoregion-based approach to protecting half the terrestrial realm. *BioScience*, 67(6):534–545, 2017. doi:10.1093/biosci/bix014.

- Ran Goldblatt, Michelle F. Stuhlmacher, Beth Tellman, Nicholas Clinton, Gordon Hanson, Matei Georgescu, Chuyuan Wang, Fidel Serrano-Candela, Amit K. Khandelwal, Wan-Hwa Cheng, and Robert C. Balling. Using landsat and nighttime lights for supervised pixel-based image classification of urban land cover. *Remote Sensing of Environment*, 205:253–275, 2018. doi:10.1016/j.rse.2017.11.026.
- E. Fairfax, E. Zhu, N. Clinton, S. Maiman, A. Shaikh, W. W. Macfarlane, and et al. Eeager: A neural network model for finding beaver complexes in satellite and aerial imagery. *Journal of Geophysical Research: Biogeosciences*, 128:e2022JG007196, 2023. doi:10.1029/2022JG007196.
- Tom Fawcett. An introduction to roc analysis. *Pattern Recognition Letters*, 27(8):861–874, 2006. ISSN 0167-8655. doi:10.1016/j.patrec.2005.10.010.
- Yuanyuan Zhao, Peng Gong, Le Yu, Luanyun Hu, Xueyan Li, Congcong Li, Haiying Zhang, Yaomin Zheng, Jie Wang, Yongchao Zhao, Qu Cheng, Caixia Liu, Shuang Liu, and Xiaoyi Wang. Towards a common validation sample set for global land-cover mapping. *International Journal of Remote Sensing*, 35(13):4795–4814, 2014. doi:10.1080/01431161.2014.930202.
- Clement Bourgoïn, Iban Amezttoy, Astrid Verhegghen, Silvia Carboni, Rene Colditz, and Frederic Achard. Global map of forest cover 2020 - version 1, 2023. URL <http://data.europa.eu/89h/10d1b337-b7d1-4938-a048-686c8185b290>. [Dataset].
- Albert W. Marshall and Ingram Olkin. A family of bivariate distributions generated by the bivariate bernoulli distribution. *Journal of the American Statistical Association*, 80(390):332–338, 1985. doi:10.2307/2287890.
- BIN DAI, SHILIN DING, and GRACE WAHBA. Multivariate bernoulli distribution. *Bernoulli*, 19(4):1465–1483, 2013. URL <http://www.jstor.org/stable/23525760>.
- Nobuyuki Otsu. A threshold selection method from gray-level histograms. *IEEE Transactions on Systems, Man, and Cybernetics*, SMC-9(1), January 1979. URL [link](#).
- N. Jean, S. Wang, A. Samar, G. Azzari, D. Lobell, and S. Ermon. Tile2vec: Unsupervised representation learning for spatially distributed data. In *Proceedings of the AAAI Conference on Artificial Intelligence*, volume 33, pages 3967–3974, 2019. doi:10.1609/aaai.v33i01.33013967.